Soft Matter

PAPER

View Article Online
View Journal

Cite this: DOI: 10.1039/d6sm00118a

Scaling dynamics of particles confined at fluid–fluid interfaces

Eduarda B. Oliveira,[a] Elton L. Correia,[a] H. Henning Winter[b] and Sepideh Razavi*[a]

Particle-laden fluid interfaces exhibit complex linear viscoelastic behavior resulting from collective particle dynamics confined to two dimensions. While interfacial rheology has been widely used to characterize such systems, a consistent framework for comparing relaxation behavior across different particle–laden interfaces remains limited. In this work, we investigate the interfacial shear rheology of hydrophobically modified silica particle monolayers at air–water and oil–water interfaces *via* small amplitude oscillatory shear measurements. Dynamic moduli obtained at different particle surface concentrations are combined into master curves *via* time–surface concentration superposition, and the viscoelastic response is analyzed in terms of relaxation time spectra obtained using the parsimonious spectral approach. The resulting spectra are well described by a truncated double power-law form analogous to the Baumgärtel–Schausberger–Winter spectrum originally developed for bulk viscoelastic materials. We refer to this representation as a two-dimensional BSW (2dBSW) spectrum and demonstrate that it captures the dominant relaxation features of the interfacial networks studied here. To further examine the scope of this approach, published interfacial rheology data for particle–laden interfaces with varying particle attributes and subphase conditions are reanalyzed within the same framework. Despite wide variations in particle type and interfacial environment in these publications, the relaxation spectra collapse onto a common self-similar form consisting of two power law columns of relaxation modes, with the longest relaxation time reflecting the strength of interparticle attractions. This apparent universality suggests that the linear viscoelastic response of particle–laden interfaces is governed by generic network features, making 2dBSW a useful and transferable description of their linear viscoelasticity.

Received 9th February 2026,
Accepted 2nd May 2026

DOI: 10.1039/d6sm00118a

rsc.li/soft-matter-journal

Introduction

The early 20th-century discovery that solid particles can stabilize emulsions and foams by adsorbing to the surfaces of droplets and bubbles laid the foundation for a field that continues to attract widespread application.[1,2] Stabilization of fluid interfaces is essential to numerous technologies, including drug delivery, food formulation, oil recovery, and personal care products.[3–10] In particle–laden interfaces, stabilization arises from a reduction in interfacial free energy, as adsorbed particles replace areas of direct contact between immiscible fluids. The energy required to desorb a particle trapped at an interface depends on the interfacial tension of the two fluids, the particle's contact angle at the interface, and its size. For colloidal particles, this desorption energy can exceed thermal energy by several orders of magnitude, resulting in effectively irreversible binding to the interface.[11–17]

In many practical systems, fluid interfaces are subjected to stresses such as compression, shear, and/or stretching. The resulting behavior depends on various particle attributes such as wettability, shape, and surface roughness. All of these particle attributes strongly affect the viscoelastic properties of interfaces.[18–21] Therefore, interfacial rheology serves as a valuable tool for characterizing such dynamics in particle–laden interfaces.[22] For instance, Van Hooghten *et al.* studied the effect of carbon black particles with engineered surface roughness at an oil–water interface.[21] They demonstrated that an enhanced lateral capillary attraction between these particles leads to the formation of strong elastic interfacial layers. By varying the volume of the spreading particle dispersion, the study further examined how rheological properties evolve with changes in surface concentration. Similarly, Beltramo *et al.* examined the dynamics of spherical polystyrene-polyvinylpyrrolidone (PS-PVP) particles at the air–water

[a] School of Chemical, Biological, and Materials Engineering, University of Oklahoma, 100 E. Boyd Street, Norman, OK 73019, USA. E-mail: srazavi@ou.edu
[b] Department of Chemical and Biomolecular Engineering and Department of Polymer Science and Engineering, University of Massachusetts Amherst, MA 01003, USA

interface at different surface coverages.[23] They reported that the elastic modulus increased with particle concentration, indicating the development of a stronger interfacial network as the interface became more densely populated. Further investigations focused on interface aging and subphase composition, identifying phenomena such as time-dependent stiffening and electrostatic screening.[24,25] Remarkably, despite the diversity of particle types and conditions studied, these rheological measurements often collapse onto master curves, pointing to universal behaviors governed by fundamental relaxation mechanisms. At sufficiently high surface coverage, particles confined to fluid–fluid interfaces experience strong geometrical constraints imposed by their neighbors. These constraints lead to transient mutual trapping of particles, – caging while being caged – and giving rise to heterogeneous dynamics characterized by a broad distribution of relaxation modes. Such caging phenomena are well known in bulk colloidal glasses, but their role in two-dimensional, interfacially confined systems is only beginning to be clarified.[26]

In a recent study, Correia *et al.* investigated monolayer assemblies of Janus particles at the air–water interface at varying surface pressures, treating their interfacial dynamics by analogy with bulk liquid behavior, as described by the well-established framework of linear viscoelasticity.[27] Drawing a parallel to the well-known time-temperature superposition principle, they introduced a time–pressure superposition approach to extend the experimental frequency range accessible *via* small-amplitude oscillatory shear (SAOS). They obtained the two-dimensional relaxation time spectrum by applying the Baumgärtel criterion.[28,29] Notably, these experimentally determined relaxation time spectra closely resemble the BSW spectrum (Baumgärtel–Schausberger–Winter model), that had previously been known to belong to some monodisperse soft materials.[30,31] The emergence of a BSW-type relaxation spectrum in these interfacial particle monolayers can be interpreted as a signature of cage-dominated dynamics.

Inspired by this approach, in this study we compare the 2D viscoelastic response of silica particle networks at the air–water and oil–water interfaces and investigate whether such a bulk-inspired model can describe the interfacial rheology of these systems, as well as other particle–laden interfaces reported in the literature. By analyzing the data through the lens of relaxation time spectra, we assess whether cage-controlled dynamics constitute a generic organizing principle for the linear viscoelastic response of particle–laden fluid interfaces, independent of particle chemistry, geometry, or subphase.

Materials and methods

Particle surface modification

Hydrophobically modified silica particles with a nominal diameter of 1 μm (Fiber Optic Center, New Bedford, MA, USA) were used in this study. The surface modification was achieved *via* silanization with dimethyldichlorosilane (DMDCS, Sigma Aldrich, St. Louis, MO, USA). The protocol involved drying 1 g of the as-received hydrophilic particles at 60 °C overnight, dispersing them in 10 mL of cyclohexane (Fisher Scientific), and sonicating the mixture with the silane reagent for 30 minutes in an ultrasonic bath (Fisherbrand™ 11203 Series, Waltham, MA, USA). The treated particles were collected by centrifugation (7000 rpm for 5 minutes, Legend X1R, Thermo Scientific) and thoroughly washed twice with cyclohexane, followed by two additional rinses with chloroform and anhydrous ethanol (Fisher Scientific). After drying under vacuum at room temperature overnight, the resulting particles – functionalized using a 10^{-4} M concentration of DMDCS – exhibited a moderate degree of hydrophobicity. All glassware was cleaned by soaking overnight in a 1 wt% KOH solution in isopropyl alcohol (Fisher Scientific) and thoroughly rinsed prior to use. Ultrapure water (18.2 MΩ cm) was obtained from a Milli-Q® IQ 7000 system (Millipore Sigma, Burlington, MA, USA) and used throughout the study.

Interfacial shear rheology measurements

To probe the mechanical response of the particle–laden interfaces, interfacial shear rheology experiments were conducted using a stress-controlled rheometer (DHR-2, TA Instruments) equipped with a double wall ring (DWR) geometry. The DWR consisted of a ring (1 mm thick) with inner and outer diameters of 69 mm and 71 mm, respectively, placed inside a double-wall cup (62 mm inner diameter, 79 mm outer diameter). The instrument was calibrated in precision mode four times to maximize sensitivity. Particle-laden monolayers were formed by first introducing 20 mL of deionized water into the DWR cup and depositing a defined volume of the particle dispersion at the air–water interface using a 50 μL Hamilton syringe. The spreading medium consisted of a particle dispersion in 70/30% ethanol/water solution at a concentration of 50 mg mL^{-1}. Particle surface concentrations were adjusted by varying the deposited volume. The applied spreading volumes of 29, 44, and 58 μL corresponded to nominal particle surface concentrations of 0.077, 0.116, and 0.154 mg cm^{-2}, respectively, calculated assuming negligible particle loss to the subphase upon deposition. After allowing 30 minutes for the spreading solvent to evaporate, the ring was gently lowered until a sharp increase in axial force indicated contact with the interface. The ring was then lowered an additional 500 μm to center it at the interface. For experiments at the oil–water interface, dodecane was carefully added atop the interface, and the system was allowed to equilibrate for 15 minutes prior to rheological testing. Oscillatory shear measurements were performed at each surface concentration. For each condition, amplitude sweeps at 0.628 rad s^{-1} were conducted to determine the linear viscoelastic regime. Frequency sweeps at 0.01% strain, well within the linear range, were performed on freshly prepared samples. The operational window for the measurements was validated using the framework proposed by Ewoldt and co-workers.[32]

2D colloidal dynamics model

The small-amplitude oscillatory shear (SAOS) data form the basis for determining the two-dimensional relaxation time

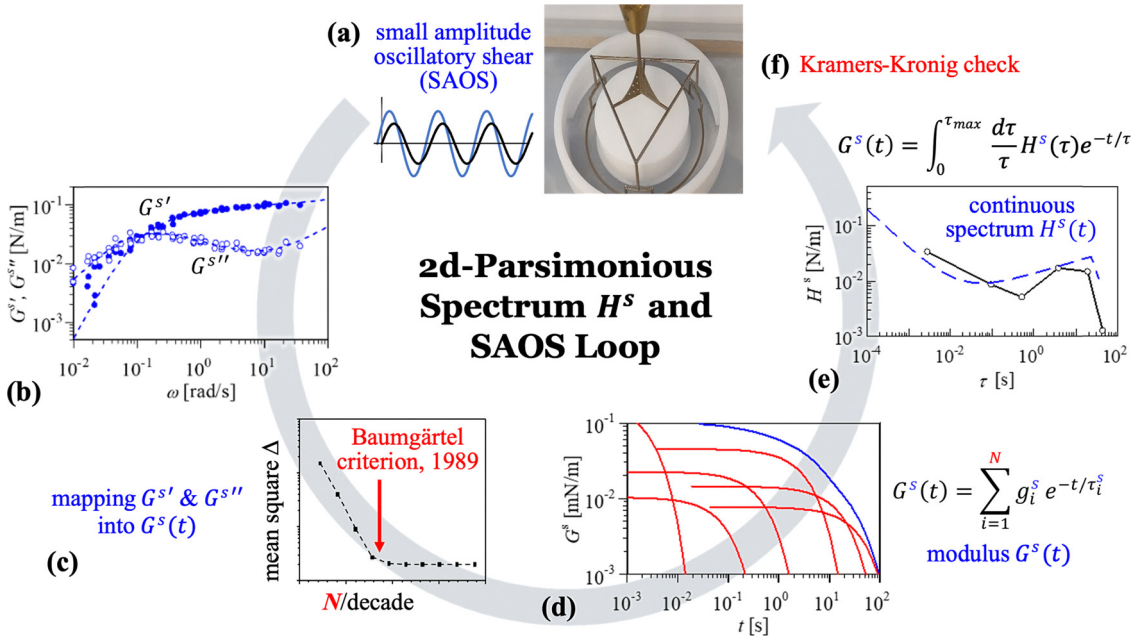

Fig. 1 Workflow for determining the 2D-parsimonious spectrum from (a) 2D-SAOS data on a particle assembly at the interface, obtained using DWR. (b) Dynamic mechanical data are (c) evaluated using the Baumgärtel criterion, (d) mapped into a discrete relaxation time spectrum with N relaxation modes, g_i^s, (e) converted into a discrete relaxation time spectrum and its corresponding continuous spectrum, and (f) tested for consistency with the Kramers–Kronig condition.[33]

spectrum. SAOS experiments (Fig. 1a) on the surface assembly yield the surface storage and loss moduli, $G^{s'}$ and $G^{s''}$ respectively, as functions of the angular frequency, ω (Fig. 1b). These dynamic moduli are related to the surface relaxation time spectrum, $H^s(\tau)$, through:

$$G^{s'}(\omega) = \int_0^{\tau_{max}} \frac{d\tau}{\tau} H^s(\tau) \frac{\omega^2\tau^2}{1+\omega^2\tau^2} \quad (1)$$

$$G^{s''}(\omega) = \int_0^{\tau_{max}} \frac{d\tau}{\tau} H^s(\tau) \frac{\omega\tau}{1+\omega^2\tau^2} \quad (2)$$

Here, τ denotes the relaxation time, τ_{max} is the upper cutoff of the relaxation time spectrum, and $H^s(\tau)$ represents the distribution of relaxation modes contributing to the interfacial response. The surface moduli vary significantly with surface pressure (Π) and surface coverage (Γ). The dynamic moduli obtained at different surface coverages can be shifted and merged into master curves (Fig. 1b), which serve as the input for mapping into a relaxation time spectrum (Fig. 1d).

The mapping procedure minimizes the deviation between the experimental data and the spectrum fit, as illustrated in the Baumgärtel plot (Fig. 1b). As shown by Baumgärtel and Winter, increasing the number of relaxation modes N improves the fit only up to a critical point, beyond which additional modes begin to represent experimental noise rather than true material behavior.[29] To avoid such overfitting, the parsimonious spectrum model identifies the optimal number of modes, N_{opt}, near this transition point, as indicated in Fig. 1c. This value is determined using the IRIS-Hub software and reflects the quality of the SAOS data, where higher noise levels typically result in a lower N_{opt}.[28]

Once the discrete spectrum is established, it is converted into a continuous relaxation time spectrum following the method of Baumgärtel and Winter, and subsequently evaluated for Kramers–Kronig consistency.[28,33]

Given the relaxation time spectrum from experiment and analysis, the stress can now be calculated for any flow, $\dot{\gamma}^s(t')$, as follows:

$$\sigma^s(t) = \int_0^{\tau_{max}} \frac{d\tau}{\tau} H^s(\tau) \int_{-\infty}^{t} dt' \dot{\gamma}^s(t') \exp\left(-\frac{t-t'}{\tau}\right) \quad (3)$$

This equation holds as long as the deformations are kept to small strains within the linear viscoelastic regime.

The viscoelastic data, as represented by the 2D parsimonious spectrum, reveal two dominant relaxation modes, which can be modeled as the linear superposition of two power laws truncated at the longest relaxation time, τ_{max}, beyond which Maxwell flow sets in (terminal zone). The resulting continuous spectrum, namely the 2dBSW spectrum, is illustrated in Fig. 2.

The complete set of parameters defining the 2dBSW spectrum consists of n_E, n_R, H_R^s, τ_R, and τ_{max}. Using these five parameters, the relaxation time spectrum can be expressed as:

$$H^s(\tau) = H_E^s \left(\frac{\tau}{\tau_E}\right)^{n_E} + H_R^s \left(\frac{\tau}{\tau_R}\right)^{-n_R} \quad (4)$$

This is valid for $\tau \leq \tau_{max}$, with the following definition applied:

$$\tau_{max} = \tau_E = \tau_R \left(\frac{H_E^s}{H_R^s}\right)^{\frac{1}{n_E}} \quad (5)$$

The ratio of characteristic times, τ_E/τ_R, quantifies the relative contributions of elastic (slow) and viscous (fast) modes.

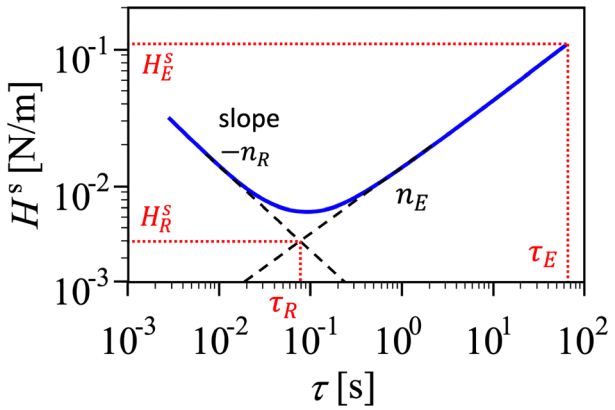

Fig. 2 Definition of the 2dBSW spectrum as linear superposition of two power laws that intersect at $H^s = H_R^s$ and $\tau = \tau_R$. The spectrum is truncated at the longest relaxation time $\tau_E = \tau_{max}$, beyond which Maxwell terminal behavior prevails. For shorter relaxation times, the spectrum follows a power law with a slope of $(-n_R)$. For longer relaxation times, it follows a power law with a slope of $(+n_E)$. The intersect of the two power law asymptotes defines the Rouse time, τ_R, as marked in the figure. In the context of interfacial particle networks, τ_R may be interpreted as a characteristic timescale of oscillatory Brownian dynamics.

A large value of this elasticity parameter indicates an interfacial monolayer dominated by elastic behavior. Together with the exponent n_E, the elasticity parameter establishes a direct relationship between the two relaxation strengths:

$$H_R^s = H_E^s \left(\frac{\tau_E}{\tau_R}\right)^{-n_E} \tag{6}$$

The two power laws intersect at $\tau = \tau_R$, where $H^s = H_R^s$.

Within a cage-based framework, the two principal branches of the 2dBSW spectrum can be interpreted as distinct modes of particle motion. The short-time power-law regime reflects localized fluctuations of particles within the transient constraints imposed by their neighbors, occurring too rapidly for stable cages to form. In contrast, the long-time regime captures cooperative restructuring processes involving cage deformation and eventual escape.

The storage modulus of the elasticity-dominated component, neglecting the viscosity-dominated contribution, is given by:

$$G^{s'}(\omega) = H_E^s \int_0^{\tau_E} \frac{d\tau}{\tau} \left(\frac{\tau}{\tau_E}\right)^{n_E} \frac{(\omega\tau)^2}{1+(\omega\tau)^2} \tag{7}$$

In the high-frequency limit, $\omega\tau_E \gg 1$, the frequency-dependent factor, $\frac{(\omega\tau)^2}{1+(\omega\tau)^2} \to 1$, saturates over the entire integration range. As a result, the storage modulus approaches a constant value and levels off into a plateau. This limiting value defines the two-dimensional plateau modulus:

$$G_N^s \equiv G^{s'}(\omega \to \infty) = \frac{H_E^s}{n_E} \tag{8}$$

The plateau modulus is a central quantity in polymer rheology, where considerable effort has been devoted to its identification and interpretation.[34] In the context of two-dimensional dynamics, it plays an equally fundamental role, emerging naturally within the 2dBSW framework as a defining material parameter. It corresponds to the asymptotic value at which the storage modulus $G^{s'}$ data levels off at high frequencies, excluding any additional upturn associated with fast modes in the spectrum. In this way, it is easily estimated from SAOS data.

The conventional BSW spectrum (three-dimensional) was originally identified as a model describing the relaxation behavior of long, linear, flexible polymers[30] and was later supported by molecular dynamics theory.[35,36] Beyond polymer melts, BSW-type spectra have also been observed in other disordered liquids composed of uniform structural constituents.[31,37–39] With the 2dBSW spectrum a steady shear viscosity can be expressed as:

$$\eta^s = \int_0^{\tau_E} d\tau H^s(\tau) = \frac{H_E^s \tau_E}{1+n_E} + \frac{H_R^s \tau_R}{1-n_R}\left(\frac{\tau_E}{\tau_R}\right)^{1-n_R} \tag{9}$$

The 2dBSW parameters were determined by modeling the experimentally determined dynamic moduli with the $G^{s'}$ and $G^{s''}$ using the constitutive expressions defined by the 2dBSW relaxation time spectrum. These expressions incorporate both power-law asymptotes, their intersection at τ_R, and truncation at the longest relaxation time, τ_E, capturing the full viscoelastic response of the interfacial assembly.

Because the integral transformations of the 2dBSW spectrum into $G^{s'}$ and $G^{s''}$ do not have closed-form analytical solutions, numerical evaluation was required. Numerical evaluation of the integral transformations and visualization of the resulting moduli were performed using the IRIS-Hub software package.[40] For a given relaxation spectrum $H^s(\tau)$, the corresponding storage and loss moduli were computed across the experimental frequency range using the standard linear viscoelastic relations described above. The discrete relaxation spectrum obtained from the experimental SAOS data was then represented using the analytical form of the 2dBSW spectrum, which is defined by five parameters (n_E, n_R, H_R^s, τ_R, and τ_E).

The parameters of the 2dBSW spectrum were determined through an iterative graphical procedure. Starting from an initial estimate of the spectral shape obtained from the calculated parsimonious relaxation spectrum, the parameters were adjusted so that the analytical 2dBSW spectrum reproduced the main features of the discrete spectrum. For each parameter set, the corresponding dynamic moduli $G^{s'}$ and $G^{s''}$ were computed and compared to the experimental SAOS data. The parameters were refined iteratively until the model curves simultaneously reproduced the discrete relaxation spectrum and the experimental frequency-dependent moduli over the full measured range.

Because both the storage and loss moduli are considered simultaneously during this comparison, the fitting procedure inherently accounts for the complete frequency-dependent viscoelastic response without preferential weighting of either modulus.

This procedure corresponds to the inspection-based fitting approach originally used in the development of the BSW spectrum for bulk viscoelastic systems, where the analytical spectrum is adjusted to reproduce the calculated relaxation spectrum and the associated dynamic moduli.[30] Because the analytical form of the 2dBSW spectrum imposes strong constraints on the spectral shape through the power-law regimes and characteristic relaxation times, the resulting parameter sets are well constrained by the experimental dynamic moduli data. In practice, the slopes of the dynamic moduli and the position of the terminal crossover strongly restrict the range of parameter combinations capable of reproducing the experimental response.

A summary of the all the experimental data sets examined in this study can be found in Table 1, whereas the values for the 2dBSW parameters obtained from this analysis are shown in Table 2 in the Results section.

Results

Experimental results

The linear viscoelastic (LVE) regime of the particle–laden interfacial networks was determined through strain amplitude sweeps, which are provided in Fig. 3a. Both the air–water and oil–water networks sustained oscillatory shear up to a strain amplitude of approximately 0.03%. However, notable differences emerged between the two systems: at comparable particle surface concentration, the storage modulus of the particle network at the air–water interface was nearly an order of magnitude greater than that at the oil–water interface, reflecting the formation of a stiffer and more elastic network. Based on these results, small-amplitude oscillatory shear (SAOS) experiments were performed at a strain amplitude of 0.01%, well within the LVE regime for both interfaces (Fig. 3b and c).

For both systems, the dynamic modulus increased systematically with particle surface concentration, consistent with the development of stronger interfacial connectivity as the interfaces became more densely populated.[23] The frequency dependence of both storage and loss moduli retained the same dual self-similar shape across surface concentrations, suggesting that the underlying relaxation mechanism remains unchanged while the overall network strength scales with surface coverage. The rheology exhibits time–(surface) concentration superposition in agreement with the previously found time–(surface) pressure superposition.[41] In order to extend the experimental frequency window, the data sets were merged into master curves *via* time–surface concentration superposition, using $\Gamma = 0.116$ mg cm^{-2} as the reference state (Fig. 4a).

The resulting master curves for both the air–water and oil–water systems exhibit the hallmark features of the 2dBSW model. The storage modulus displayed a downward curvature towards low frequencies, while the loss modulus rose with decreasing frequency before reaching a maximum and subsequently declining. A key distinction between the two systems lies in the slope of the loss modulus as it increases towards lower frequencies, a difference that becomes more pronounced when examining the corresponding relaxation time spectra (Fig. 4b). These behaviors are consistent with the presence of multiple relaxation modes spanning a broad range of timescales, as captured by the 2dBSW framework. These results suggest that a common set of fundamental relaxation processes govern the viscoelastic response of particle-stabilized networks, despite differences in the magnitude of their elastic and viscous moduli.

Applicability of 2dBSW spectra to published SAOS data

The foundation for the present analysis lies in the work of Correia *et al.*, who first demonstrated that interfacial SAOS data could be interpreted through a relaxation spectrum analogous to that of three-dimensional BSW framework.[41] This finding established that the underlying spectral organization is independent of spatial dimensionality. Oliveira *et al.* extended this approach to particle–laden oil–water interfaces, demonstrating that the 2dBSW framework applies and sensitively distinguishes the dynamics of silica particles of differing wettability.[42] They found that, despite differences in particles degree of hydrophobicity and the resulting interfacial network structure, the frequency sweeps collapsed onto master curves analogous to BSW-type dynamics. Encouraged by these findings, we formalize the 2dBSW relaxation spectrum and examine its broader applicability to particle–laden interfaces across a wide range of particle size, shape, roughness, chemistry, and

Table 1 Summary of literature data analyzed. Information is provided on the type and size of the particles examined, the fluids used in the interfacial assembly, and the technique utilized in the characterization of the networks' interfacial rheology

Authors	Year	Particles	Interface	Method
Correia *et al.*[41]	2023	Silica/gold Janus particles (D = 1 μm)	Air/water	Stress-controlled rheometer equipped with a DWR geometry
van den Berg *et al.*[24]	2018	Cellulose nanocrystals (rod-like particles with D = 5–7 nm and L = 50–3000 nm)	Air/water	Stress-controlled rheometer equipped with a bicone geometry
Zhang *et al.*[25]	2016	Hydrophobic silica nanoparticles (D = 34 nm)	Air/aqueous (5 mM to 2 M Na_2SO_4)	Stress-controlled rheometer equipped with a DWR geometry
Oliveira *et al.*[42]	2026	Hydrophobic silica particles (D = 1 μm)	Dodecane/water	Stress-controlled rheometer equipped with a DWR geometry
van Hooghten *et al.*[21]	2013	Rough carbon black particles ($D_{H,CB1}$ = 62 nm and $D_{H,CB2}$ = 33 nm)	*n*-octane/aqueous (0.05 M NaCl)	Stress-controlled rheometer equipped with a DWR geometry
Beltramo *et al.*[23]	2017	Polystyrene-polyvinylpyrrolidone spheres (D = 820 nm)	Air/water	Stress-controlled rheometer equipped with a DWR geometry

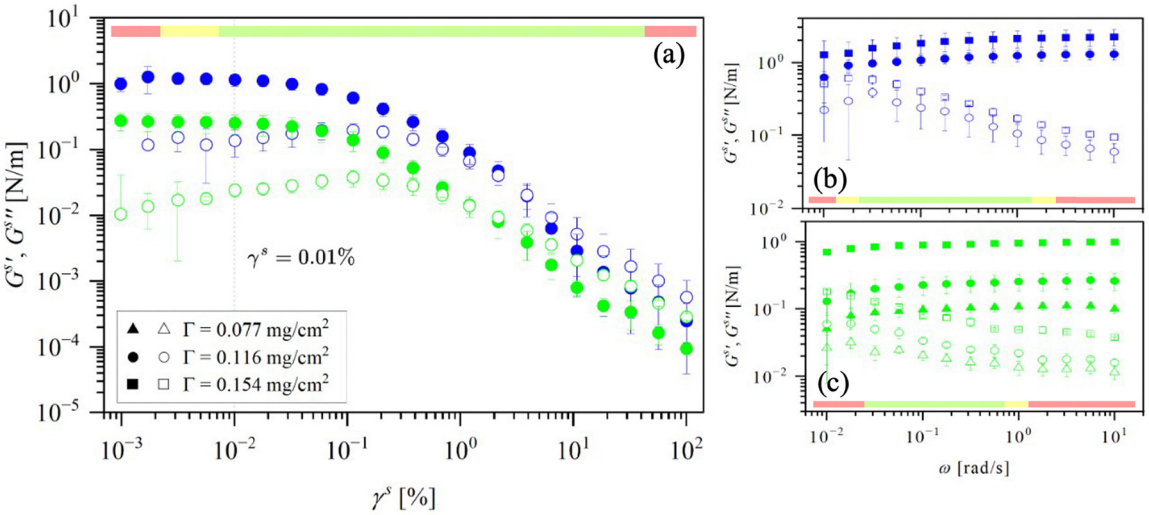

Fig. 3 (a) Amplitude sweeps (ω = 0.628 rad s^{-1}) for hydrophobically modified silica particles at a surface concentration of 0.116 mg cm^{-2} deposited at the air–water interface (blue) and oil–water interface (green). Frequency sweeps (γ^s = 0.01%) at varying particle surface concentrations for particle networks formed at (b) the air–water interface and (c) oil–water interface. Solid and open symbols represent the elastic modulus and viscous modulus, respectively. Color coded operating window is as follows: green range represents an acceptable data set, yellow range represents probably acceptable data, and the data in the red range needs to be handled with care.

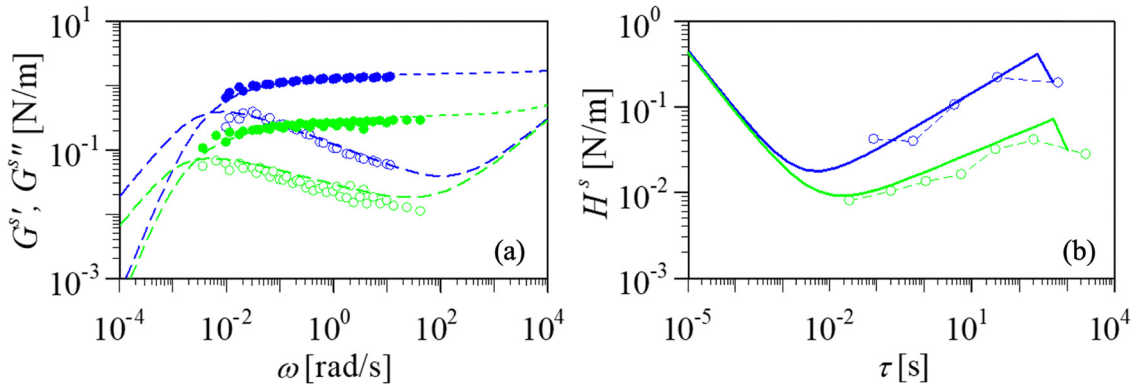

Fig. 4 (a) Master curve for surface elastic modulus (solid symbols) and surface viscous modulus (open symbols) obtained from hydrophobically modified silica particles at the air–water interface (blue) and oil–water interface (green) using the reference state (Γ = 0.116 mg cm^{-2}). (b) Corresponding relaxation time spectra, where symbols represent the parsimonious spectra and solid lines represent the continuous self-similar 2dBSW spectra.

subphase composition. To this end, we reanalyze published SAOS data within the 2dBSW framework, assessing the presence of its characteristic relaxation signatures. A summary of the literature data analyzed here can be found in Table 1.

Janus particles at the air–water interface (Correia *et al.*, 2023)[41]. The Janus particles – 1 μm silica with gold-coated, thiol-functionalized hemisphere – formed monolayers whose dynamic moduli increased with surface pressure while maintaining the same frequency dependence.[41] Through time–pressure superposition, the data collapsed into a master curve, allowing the extraction of a relaxation spectrum, a precursor to what we here define as the 2dBSW spectrum (Fig. 5). The resulting $G^{s'}$ and $G^{s''}$ profiles show all key signatures of the 2dBSW model, capturing both the low-frequency cutoff pattern associated with the longest relaxation time and the onset of the high-frequency loss modulus upturn. This suggests that the 2dBSW framework can accurately describe viscoelastic dynamics of particle–laden fluid interfaces.

Shape anisotropic particles at the air–water interface (van den Berg *et al.*, 2018)[24]. Inspired by this initial demonstration, we apply the same framework to an interface laden with shape anisotropic particles. The cellulose nanocrystals (CNCs) studied by van den Berg *et al.* had a rod-like shape, introducing orientation-dependent interactions that dictate network structure and rheological behavior at the air–water interface.[24] Their alignment, rotation, and steric hinderance add new pathways for stress dissipation, with the resulting networks undergoing significant time-dependent stiffening. The interfacial mechanics were characterized using frequency sweeps performed at different surface layer aging times, capturing the

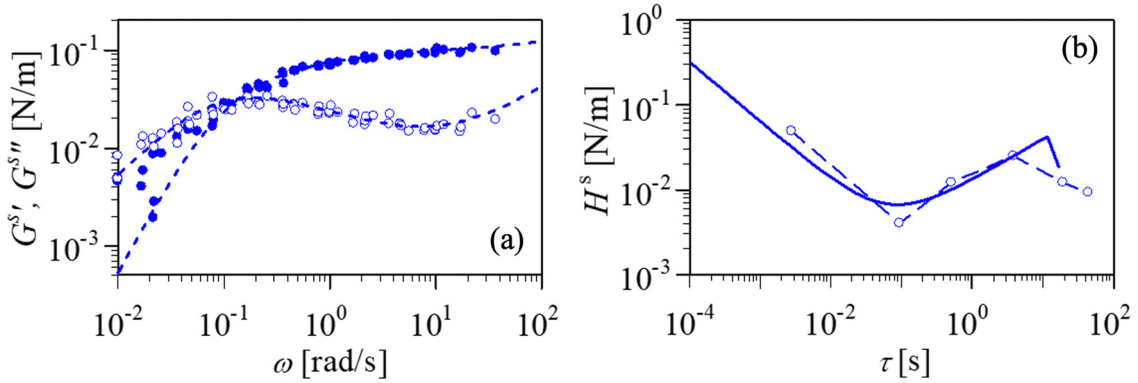

Fig. 5 Correia *et al.* (2023); (a) master curve for network of Janus particles at the air–water interface. (b) Corresponding relaxation time spectrum, where symbols represent the parsimonious spectrum and the solid line represents the continuous 2dBSW spectrum. The reference state used in shifting the data is Π = 30 mN m^{-1}. Adapted from ref. 41.

evolution of the viscoelastic response. Despite this evolving microstructure, the SAOS data collapsed into master curves through time-dependent shifting, and the extracted relaxation spectra remained consistent with 2dBSW model (Fig. 6). This indicates that the framework remains applicable even for anisotropic systems with complex aging behavior.

Nanoparticles under varying electrolyte concentration (Zhang *et al.*, 2016)[25]. Beyond particle geometry, network formation and its resulting dynamics are also influenced by the fluid phases composing that interface. In the work of Zhang *et al.* (2016), electrostatics plays a key role in the behavior of 34 nm silica nanoparticles at the air–water interface under varying electrolyte concentrations. Increasing ionic strength suppressed electrostatic repulsion, allowing stronger interfacial association and enhanced viscoelastic response.[25] The interfacial dynamics were probed using SAOS measurements, specifically frequency sweeps were performed at different salt concentrations while maintaining the same particle deposited amount. When re-analyzed within the 2dBSW framework, the frequency-dependent moduli collapse into master curves through electrolyte-based shifting and yield relaxation spectra that follow the same characteristic trends observed in Correia and van den Berg (Fig. 7). This demonstrates that while changes in the subphase chemistry modulate the network mechanics, the 2dBSW model's predictive framework remains valid.

Hydrophobic silica particles at the oil–water interface (Oliveira *et al.*, 2026)[42]. Having shown that the same underlying viscoelastic signatures emerge across variations in particle geometry and subphase chemistry at air–water interfaces, we now turn to a different fluid–fluid boundary. Oliveira *et al.* examined silica particles of varying wettability at the oil–water interface using the same spectral analysis approach introduced by Correia.[41,42] The silica particles were hydrophobically modified to different extents, yielding particles with estimated oil–water contact angles of ∼85° and ∼150°. Frequency sweeps at different particle surface concentrations revealed distinct viscoelastic signatures for the two particle types, yet in both cases the data collapsed onto master curves *via* time–surface concentration superposition (Fig. 8). These results further support the idea that a common set of fundamental relaxation processes governs the viscoelasticity of particle-stabilized fluid interfaces across different fluid–fluid

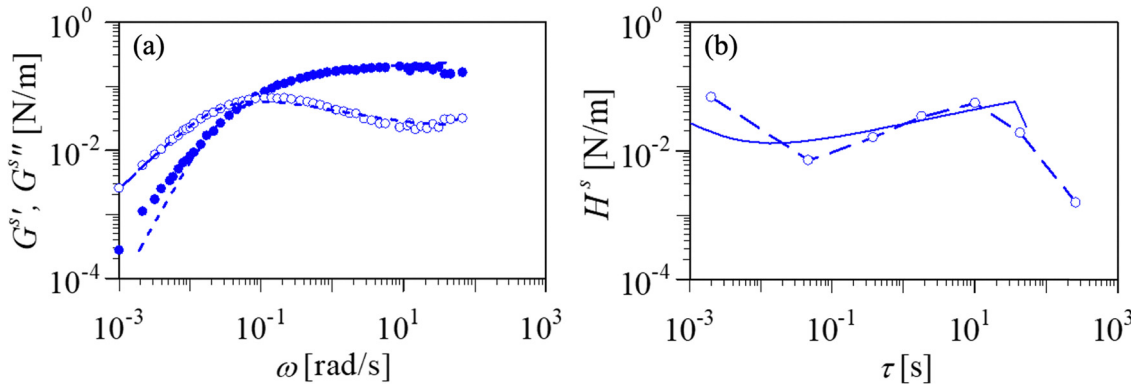

Fig. 6 van den Berg *et al.* (2018); (a) master curve for network of cellulose nanocrystals at the air–water interface. (b) Corresponding relaxation time spectrum, where symbols represent the parsimonious spectrum and the solid line represents the continuous 2dBSW spectrum. The reference state is t = 38 hours. SAOS data were digitized from published measurements reported in ref. 24 and replotted here to construct the master curve and relaxation spectrum using the analysis described in this work.

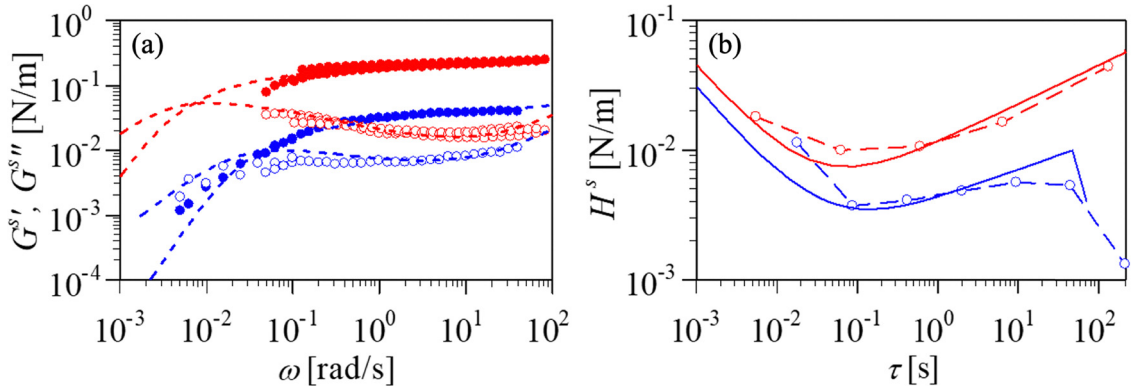

Fig. 7 Zhang *et al.* (2016); (a) master curve for silica nanoparticle at the air–water interface at high subphase salt concentrations (red) and low subphase salt concentrations (blue). (b) Corresponding relaxation time spectra, where symbols represent the parsimonious spectra and solid lines represent the continuous 2dBSW spectra. The reference states are 50 mM (red) and 7 mM (blue) salt subphase concentrations. SAOS data were digitized from published measurements reported in ref. 25 and replotted here to construct master curves and relaxation spectra using the analysis described in this work.

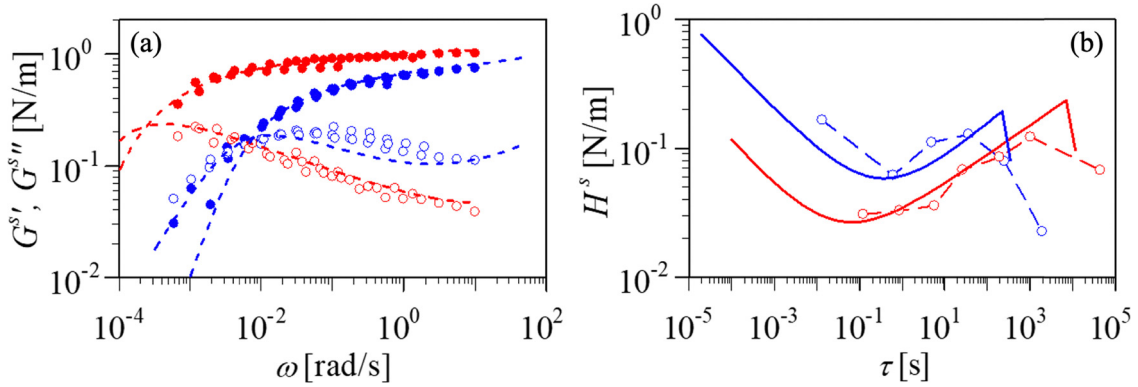

Fig. 8 Oliveira *et al.* (2026); (a) master curves for hydrophobically modified silica particles (red – CA ~85° and blue – CA ~150°) at the oil–water interface. (b) Corresponding relaxation time spectra, where symbols represent the parsimonious spectra and solid lines represent the continuous 2dBSW spectra. The reference state is Γ = 0.154 mg cm^{-2} for both particle types. Adapted from ref. 42.

boundaries. However, limitations arising from the restricted experimental frequency window became more evident: the low-frequency cutoff was captured only for one particle type, suggesting that the maximum in $G^{s\prime\prime}(\omega)$ likely occurs at frequencies lower than the accessible range. Likewise, the high-frequency upturn associated with fast, local dissipation mechanisms that was observed for Janus particles was not resolved here. Consequently, the extracted spectra emphasized long relaxation modes, with diminished information on fast dynamics.

Rough particles at the oil–water interface (van Hooghten *et al.*, 2013)[21]. Additional insight into the role of particle attributes comes from systems with more limited accessible frequency ranges. Van Hooghten *et al.* compared carbon black (CB) particles of different nanoscale roughness at the octane-water interface.[21] Both particle types formed strong, elastic networks through lateral capillary interactions, with elasticity increasing with surface concentration. When interpreted within the 2dBSW framework, the data collapse into master curves and yield relaxation spectra that capture the dominant long-time relaxation modes (Fig. 9). However, the experimentally accessible frequency window does not extend to sufficiently low frequencies to resolve the downturn in $G^{s\prime\prime}(\omega)$ or the crossover frequency associated with the longest relaxation time. As a result, while roughness-dependent differences in interfacial mobility are still evident through variations in the magnitude of H^s, the full low-frequency structure of the spectrum cannot be directly assessed. Although the experimental frequency window is restricted, the data remains compatible with the 2dBSW description. This example illustrates how particle morphology can be meaningfully compared within the 2dBSW framework, even when key spectral features lie outside the measurable range.

Spherical particles at the air–water interface (Beltramo *et al.*, 2017)[23]. The influence of experimental constraints on spectral interpretation is further illustrated by the work of Beltramo *et al.*, who examined the behavior of spherical polystyrene-polyvinylpyrrolidone (PS-PVP) particles (D = 820 nm) at the air–water interface.[23] Increasing surface coverage systematically enhanced the surface elastic modulus, indicating progressive network strengthening as the interface becomes more densely

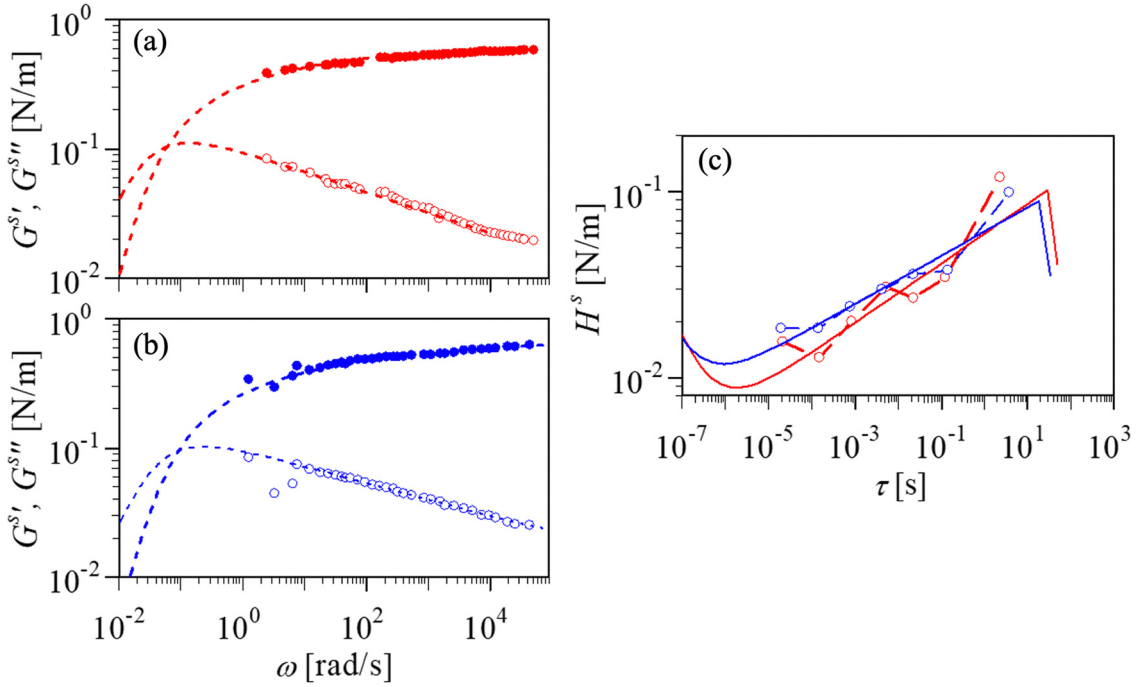

Fig. 9 van Hooghten *et al.* (2013); (a) master curve for CB1 (red) particles, (b) master curve for CB2 (blue) particles, as presented in the original work. (c) Corresponding relaxation time spectra, where symbols represent the parsimonious spectra and solid lines represent the continuous 2dBSW spectra. Adapted from ref. 21.

populated (Fig. 10). When recast into 2dBSW framework, their data collapses into a master curve with a limited frequency window and relatively considerable noise levels. While this data alone does not permit definitive conclusions, its qualitative consistency with the 2dBSW framework underscores both the potential generality of the model and the critical importance of high-quality, broad-band rheological measurements.

Parameters of the 2dBSW spectrum

The empirical 2dBSW spectrum used in this work is defined by five parameters: H_R^s, τ_R, τ_E, τ_R, and n_E. The most dominant 2dBSW features are what sometimes is called the alpha relaxation consisting of a power law with positive exponent n_E, lead relaxation strength H_E^s and a longest relaxation time τ_E:

$$H^s(\tau) \approx H_E^s \left(\frac{\tau}{\tau_E}\right)^{n_E} \quad \text{for } \tau < \tau_E \tag{10}$$

From a physical standpoint, the α-relaxation represents the slowest structural rearrangements of the interfacial particle network and can be associated with cage-breaking events, in which particles collectively escape their local constraints. Accordingly, the longest relaxation time, τ_E, can be viewed as an effective escape time, characterizing the lifetime of load-bearing particle cages before collective rearrangement. In

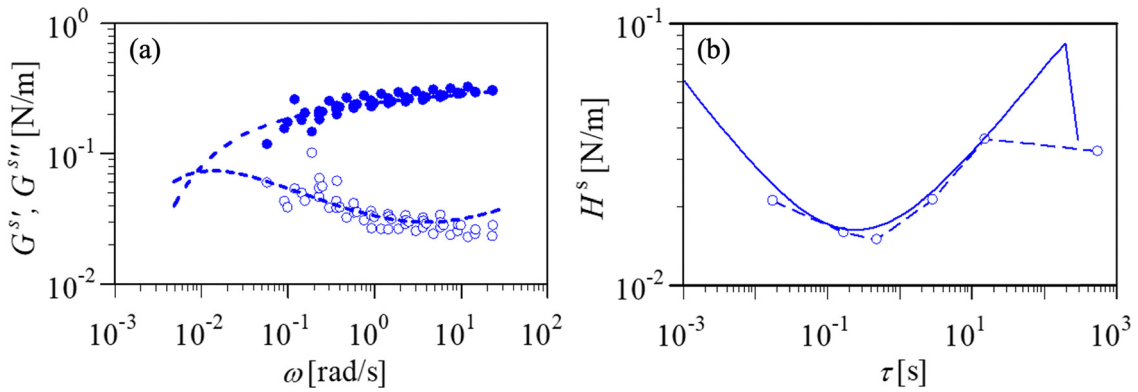

Fig. 10 Beltramo *et al.* (2017); (a) master curve for PS-PVP particles at the air–water interface. (b) Corresponding relaxation time spectrum, where symbols represent the parsimonious spectrum and the solid line represents the continuous 2dBSW spectrum. The reference state is 71% surface coverage by particles. SAOS data were digitized from published measurements reported in ref. 23 and replotted here to construct the master curve and relaxation spectrum using the analysis described in this work.

Table 2 2dBSW fitting parameters for analyzed literature data. The 'Condition' column distinguishes multiple datasets within a given reference; studies reporting a single dataset are labeled as 'Single condition.'

Author	Condition	n_E	n_R	H_R^s [Pa m]	τ_R [s]	H_E^s [Pa m]	τ_E [s]
Correia *et al.*(Fig. 5)	Single condition	0.3	0.7	3.31×10^{-3}	8.52×10^{-3}	3.32×10^{-2}	18.6
van den Berg *et al.*(Fig. 6)	Single condition	0.23	0.7	5.00×10^{-3}	5.37×10^{-3}	4.14×10^{-2}	52.5
Zhang *et al.* (Fig. 7)	Subphase with low salt	0.23	0.73	2.34×10^{-3}	6.60×10^{-2}	1.18×10^{-2}	75.8
	Subphase with high salt	0.3	0.7	4.17×10^{-3}	2.95×10^{-2}	7.13×10^{-2}	380
Oliveira *et al.* (Fig. 8)	S1 (high hydrophobicity)	0.28	0.34	2.75×10^{-2}	1.70×10^{-1}	2.26×10^{-1}	316
	S4 (moderate hydrophobicity)	0.23	0.37	1.26×10^{-2}	3.90×10^{-2}	2.67×10^{-1}	2290
van Hooghten *et al.* (Fig. 9)	CB1 (greater roughness)	0.16	0.7	4.16×10^{-3}	5.37×10^{-8}	1.13×10^{-1}	48.9
	CB2 (lower roughness)	0.13	0.7	6.60×10^{-3}	5.37×10^{-8}	9.19×10^{-2}	33.8
Beltramo *et al.* (Fig. 10)	Single condition	0.35	0.37	8.88×10^{-3}	2.33×10^{-1}	8.16×10^{-1}	289

SAOS, this manifests as a steady increase of $G^{s''}$ toward low frequencies, accompanied by a decay of $G^{s'}$, with the two moduli converging near $\omega = 1/\tau_E$ and subsequently decaying.

High frequency data are notoriously difficult to gain from experiments. Nevertheless, when the SAOS frequency window is sufficiently broad, all five parameters of the 2dBSW spectrum can be extracted: the prefactor H_R^s sets the overall magnitude of the spectrum, while τ_R marks the intersection of the two power-law branches and may be interpreted as a short-time Brownian particle motion. The exponents n_R and n_E define the slopes of the short-time and long-time branches of the relaxation spectrum, respectively, thereby capturing the apparent broadness and asymmetry of the spectrum. The longest relaxation time, τ_E, introduces the low-frequency cutoff and corresponds to the slowest relaxation process of the particle interface. While the exponents n_R and n_E encode the apparent breadth and asymmetry of the relaxation spectrum, their precise physical interpretation in terms of cage geometry or dynamical heterogeneity remains limited by experimental bandwidth and data quality.

The identifiability of the 2dBSW parameters depends strongly on the width of the accessible frequency window and data quality. Most robustly resolved in SAOS data is the low-frequency scaling exponent n_E, reflected in the slope of $G^{s''}$ at intermediate frequencies. Limited low-frequency resolution constrains estimates of τ_E, while the absence of a clear high-frequency upturn restricts the determination of τ_R and n_R. As a result, some parameters may appear similar across systems simply due to bandwidth limitations rather than true dynamical similarity. Table 2 summarizes the fitted 2dBSW parameters extracted for each dataset analyzed in this work, providing a basis for the comparisons that follow.

Discussion

The agreement between the experimental results of Correia *et al.* and Oliveira *et al.* sets the stage for the present investigation. These two examples illustrate a central point: despite clear differences in particle chemistry and interfacial environment, both systems conform to the same 2dBSW-type spectral form. The underlying structure is thus independent of microscopic detail, while the measurable response remains sensitive to it. The repeated observation of a 2dBSW-type spectrum across such disparate systems indicates that cage-controlled dynamics follows a universal scaling organization. This organization is defined by the two mirrored 2dBSW power-law cascades of relaxation modes, which appear as a generic feature of particle–laden interfaces. In this sense, the 2dBSW spectrum provides a universal framework for describing linear viscoelasticity in two dimensions. At the same time, the parameters of the 2dBSW spectrum are not universal. They depend on system-specific details such as particle interactions, wettability, and interfacial structure. The framework is therefore universal in form but material-specific in its parameters – a distinction that was examined throughout the reviewed literature data.

Motivated by this apparent universality, we examined published 2D shear viscoelasticity data spanning a broad range of particle–laden interfaces. The datasets encompass variations in particle shape, size, roughness, and surface chemistry, as well as differences in interfacial environment, including air–water *versus* oil–water interfaces and the presence or absence of salts in the subphase. These factors are known to influence interparticle interactions, network formation and dynamics, and thus to affect the distribution of relaxation times. For example, surface roughness and shape anisotropy promote jamming at the interface, increasing elasticity and broadening the relaxation spectrum (Fig. 9), while surface chemistry (Fig. 8) and subphase composition (Fig. 7) modify electrostatic interactions and shift the distribution of fast and slow relaxation processes. Importantly, while these attributes modulate the strength and stability of particle cages, they do not appear to alter the underlying hierarchy of relaxation processes encoded in the 2dBSW spectrum.

Beyond qualitative similarities, the 2dBSW fitting results identify a parameter with clear physical significance: the longest relaxation time, τ_E. The parameter τ_E represents the terminal timescale of the relaxation hierarchy and corresponds to the slowest structural rearrangements of the interfacial network. In particle–laden interfaces, particles are confined to a quasi-two-dimensional environment and interact through capillary, van der Waals, and/or electrostatic forces, leading to transient cages formed by neighboring particles. Within this framework, τ_R reflects local relaxation associated with particle fluctuations within these cages, whereas τ_E corresponds to the timescale required for cooperative rearrangements that enable particles to escape their local confinement. Because such events involve the coordinated motion of multiple particles,

τ_E is more appropriately interpreted as a collective restructuring time of the interfacial network rather than a simple bond lifetime. This interpretation is consistent with the trends observed across the datasets.

Across systems, τ_E consistently reflects the relative strength of attractive interactions within the interfacial network. Interfaces dominated by strong attraction exhibit larger τ_E, corresponding to slower structural rearrangements and more persistent load-bearing configurations, whereas more weakly interacting or predominantly repulsive systems display shorter τ_E and faster relaxation pathways. For example, τ_E increases from approximately 76 s to 380 s with increasing salt concentration in the subphase for the interfacial particle network studied by Zhang *et al.*, consistent with enhanced attractive interparticle interactions due to electrostatic screening (Table 2). A similar trend is observed for particles of varying hydrophobicity in Oliveira *et al.*, where τ_E increases from 316 s to 2290 s, reflecting stronger capillary interactions in the latter case, and a greater resistance to cooperative rearrangement (Table 2). Similarly, Correia *et al.* has shown that τ_E scales with surface pressure (*i.e.*, surface packing density of particles), with τ_E increasing from approximately 10 s at $\Pi = 5$ mN m^{-1} to 45 s at $\Pi = 50$ mN m^{-1}.[41] Taken together, these observations suggest that τ_E primarily captures the combined effects of interaction strength and degree of confinement within the interfacial network.

However, extending this interpretation across different systems reveals an additional contribution. For instance, both the hydrophobically modified silica particles studied by Oliveira *et al.* (Fig. 4) and the rough carbon black particles of van Hooghten *et al.* (Fig. 9) form strongly attractive interfacial networks and exhibit similar 2dBSW spectral shapes. Despite this, τ_E differs by orders of magnitude, with significantly larger values in the Oliveira systems (Table 2). While wettability variations within this system lead to systematic changes in τ_E (316–2290 s), the much smaller range of τ_E for nanoscale carbon black particles (34–49 s) indicates that additional factors contribute to relaxation across systems. In particular, hydrodynamic interactions introduce viscous resistance to particle motion and modify the rate of restructuring at interfaces, as shown in simulations by Dani *et al.*[43] The larger particle size of the hydrophobically modified silica particles studied by Oliveira *et al.* (micron-scale) compared to the nanoscale carbon black particles of van Hooghten *et al.* is expected to increase hydrodynamic resistance to particle motion. In addition, differences in the oil phase further contribute to this effect: in the systems studied by Oliveira *et al.* dodecane is used as the oil phase, which is more viscous than the octane used by van Hooghten *et al.*, leading to greater viscous dissipation during interfacial rearrangements. Together, the increased particle size and higher oil viscosity enhance hydrodynamic interactions, slowing cooperative rearrangements and shifting τ_E to longer times. Importantly, these effects alter the relaxation timescales without changing the underlying 2dBSW scaling structure.

While τ_E provides a consistent and physically meaningful measure of relaxation dynamics, the interpretation of the remaining spectral parameters is more sensitive to experimental resolution and fitting constraints and must therefore be made with caution. A critical limitation of the existing literature is the restricted quality and scope of many datasets. Narrow frequency windows, experimental noise, and limited resolution often constrain the number of resolvable relaxation modes. Under such conditions, the relaxation spectrum captures only the dominant dynamical features, while finer details remain unresolved. In particular, insufficient high-frequency data restricts determination of τ_R and n_R. As a result, apparent similarities in these parameters may reflect experimental limitations rather than true dynamical equivalence. This highlights that, while the 2dBSW form captures the overall structure of the relaxation spectrum, not all parameters are equally reliable for physical interpretation. Nevertheless, the 2dBSW framework enables consistent comparison across systems, even when the original analyses employed different rheological representations, revealing common spectral features that might otherwise remain obscured.

The observed hierarchy of relaxation processes can be further interpreted within the SCOPE (spectral classification of processes and eigenmodes) framework.[43] High-frequency modes are governed by short-time relaxation processes associated with intra-cage particle motion that rapidly equilibrates local stresses, while low-frequency modes reflect long-time relaxation processes corresponding to cooperative rearrangements of the interfacial network. Within this picture, cage escape emerges as a delayed, collective process governed by the gradual buildup and release of elastic stresses, consistent with the interpretation of τ_E as a restructuring timescale of the interface. Experimentally, these regimes are reflected in the frequency dependence of the dynamic moduli: short-time intracage dynamics dominate the high-frequency response, whereas the approach to τ_E is marked by the convergence of $G^{s'}$ and $G^{s''}$ and the onset of terminal relaxation behavior. Although the relative magnitudes of $G^{s'}$ and $G^{s''}$ depend on the specific system and frequency range, the SCOPE framework provides a useful link between the distribution of relaxation modes and observable rheological features.

Thus, our analysis shows that while particle properties and subphase conditions modulate the quantitative viscoelastic response, the 2dBSW spectrum captures the dominant relaxation behavior across a wide range of particle–laden interfaces. This apparent universality has important practical implications: it suggests that the linear viscoelastic properties of interfacial particle networks may be predicted from general features of caging and network formation, rather than requiring system-specific characterization in every case. Future progress will depend on high-quality experimental data with extended frequency coverage to fully resolve relaxation spectra and delineate the limits of this presumed universality. Systematic variation of particle properties, combined with reduced noise and broader dynamic windows, will further clarify the mechanisms governing relaxation in 2D interfacial systems and support the rational design of interfaces with tailored viscoelastic performance.

Conclusions

In this work, we demonstrated that the relaxation spectra of particle–laden fluid interfaces can be successfully captured by the 2dBSW framework. Application of this model to both our experimental data and to selected literature studies revealed striking similarities in the spectral features of diverse particle systems, despite variations in particle size, shape, wettability, and subphase. These findings suggest that the viscoelastic response of particle-stabilized interfaces may follow a universal rheological pattern, paralleling the behavior observed in bulk three-dimensional systems. At the same time, our analysis highlights important challenges. While the approach proved robust, the extraction of relaxation spectra can be hindered by experimental noise and by the relatively narrow frequency windows typical of interfacial rheology measurements, both of which limit the resolution of spectral features.

Altogether, the present results establish the 2dBSW model as a powerful tool for probing the viscoelasticity of particle–laden interfaces and open the door to a unified framework for describing two-dimensional interfacial rheology. Future studies that directly link relaxation modes to microscopic particle dynamics – measuring cage size, lifetime, and heterogeneity through particle tracking or scattering – will be essential to establish a quantitative connection between the 2dBSW parameters and interfacial caging dynamics.

Conflicts of interest

The authors declare no competing interests.

Data availability

The data supporting the findings of this study are available from the corresponding author upon request.

Acknowledgements

SR and EO acknowledge the support from the National Science Foundation through the NSF-CAREER award CBET-2144020. HHW acknowledges the support of the U.S. Department of Energy, Office of Energy Efficiency and Renewable Energy, Bioenergy Technologies Office under Award Number DEEE0009285. The data analysis, modelling, and plotting was done with IRIS Rheo-Hub software (https://rheology.tripod.com/General_Description_of_IRIS.pdf).

References

1 W. Ramsden, Separation of solids in the surface-layers of solutions and 'suspensions' (observations on surface-membranes, bubbles, emulsions, and mechanical coagulation).—Preliminary account, *Proc. R. Soc. London*, 1904, **72**(477–486), 156–164, DOI: 10.1098/rspl.1903.0034.

2 S. U. Pickering, CXCVI.—Emulsions, *J. Chem. Soc., Trans.*, 1907, **91**(0), 2001–2021, DOI: 10.1039/ct9079102001.

3 R. Aveyard, B. P. Binks and J. H. Clint, Emulsions stabilised solely by colloidal particles, *Adv. Colloid Interface Sci.*, 2003, **100–102**, 503–546, DOI: 10.1016/S0001-8686(02)00069-6.

4 B. P. Binks and T. S. Horozov, *Colloidal Particles at Liquid Interfaces*, Cambridge University Press, 2006. , DOI: 10.1017/CBO9780511536670.

5 S. Crossley, J. Faria, M. Shen and D. E. Resasco, Solid Nanoparticles that Catalyze Biofuel Upgrade Reactions at the Water/Oil Interface, *Science*, 2010, **327**(5961), 68–72, DOI: 10.1126/science.1180769 (acccessed 2024/06/05).

6 A. J. Mendoza, E. Guzmán, F. Martínez-Pedrero, H. Ritacco, R. G. Rubio, F. Ortega, V. M. Starov and R. Miller, Particle laden fluid interfaces: Dynamics and interfacial rheology, *Adv. Colloid Interface Sci.*, 2014, **206**, 303–319, DOI: 10.1016/j.cis.2013.10.010.

7 B. P. Binks, Colloidal Particles at a Range of Fluid–Fluid Interfaces, *Langmuir*, 2017, **33**(28), 6947–6963, DOI: 10.1021/acs.langmuir.7b00860.

8 C. Chen, S. Wang, M. J. Kadhum, J. H. Harwell and B.-J. Shiau, Using carbonaceous nanoparticles as surfactant carrier in enhanced oil recovery: A laboratory study, *Fuel*, 2018, **222**, 561–568, DOI: 10.1016/j.fuel.2018.03.002.

9 R. Liu, A. K. Y. Raman, I. Shaik, C. Aichele and S.-J. Kim, Inorganic microfiltration membranes incorporated with hydrophilic silica nanoparticles for oil-in-water emulsion separation, *J. Water Process Eng.*, 2018, **26**, 124–130, DOI: 10.1016/j.jwpe.2018.10.002.

10 C. Qian, A. Telmadarreie, M. Dong and S. Bryant, Synergistic Effect between Surfactant and Nanoparticles on the Stability of Foam in EOR Processes, *SPE J.*, 2020, **25**(02), 883–894, DOI: 10.2118/195310-pa.

11 B. P. Binks, Particles as surfactants—similarities and differences, *Curr. Opin. Colloid Interface Sci.*, 2002, **7**(1), 21–41, DOI: 10.1016/S1359-0294(02)00008-0.

12 B. J. Park and D. Lee, Particles at fluid–fluid interfaces: From single-particle behavior to hierarchical assembly of materials, *MRS Bull.*, 2014, **39**(12), 1089–1098, DOI: 10.1557/mrs.2014.253 (acccessed 2024-06-06T14:59:32).

13 D. Y. Zang, E. Rio, D. Langevin, B. Wei and B. P. Binks, Viscoelastic properties of silica nanoparticle monolayers at the air-water interface, *Eur. Phys. J. E:Soft Matter Biol. Phys.*, 2010, **31**(2), 125–134, DOI: 10.1140/epje/i2010-10565-7 (acccessed 2024-06-06T14:58:59).

14 A. Böker, J. He, T. Emrick and T. P. Russell, Self-assembly of nanoparticles at interfaces, *Soft Matter*, 2007, **3**(10), 1231, DOI: 10.1039/b706609k (acccessed 2024-06-06T14:58:32).

15 S. Komura, Y. Hirose and Y. Nonomura, Adsorption of colloidal particles to curved interfaces, *J. Chem. Phys.*, 2006, **124**(24), 241104, DOI: 10.1063/1.2216697 (acccessed 2024-06-06T14:57:28).

16 E. M. Furst, Directing colloidal assembly at fluid interfaces, *Proc. Natl. Acad. Sci. U. S. A.*, 2011, **108**(52), 20853–20854, DOI: 10.1073/pnas.1118441109 (acccessed 2024-06-06T14:58:04).

17 F. Bresme and M. Oettel, Nanoparticles at fluid interfaces, *J. Phys.: Condens. Matter*, 2007, **19**(41), 413101, DOI: 10.1088/0953-8984/19/41/413101 (acccessed 2024-06-06T14:56:48).

18 K. Yu, H. Zhang, S. Biggs, Z. Xu, O. J. Cayre and D. Harbottle, The rheology of polyvinylpyrrolidone-coated silica nanoparticles positioned at an air-aqueous interface, *J. Colloid Interface Sci.*, 2018, **527**, 346–355, DOI: 10.1016/j.jcis.2018.05.035.

19 J. H. J. Thijssen and J. Vermant, Interfacial rheology of model particles at liquid interfaces and its relation to (bicontinuous) Pickering emulsions, *J. Phys.: Condens. Matter*, 2018, **30**(2), 023002, DOI: 10.1088/1361-648x/aa9c74 (acccessed 2024-07-29T20:39:24).

20 E. L. Correia, N. Brown and S. Razavi, Janus Particles at Fluid Interfaces: Stability and Interfacial Rheology, *Nanomaterials*, 2021, **11**(2), 29, DOI: 10.3390/nano11020374, Review.

21 R. Van Hooghten, L. Imperiali, V. Boeckx, R. Sharma and J. Vermant, Rough nanoparticles at the oil–water interfaces: their structure, rheology and applications, *Soft Matter*, 2013, **9**(45), 10791, DOI: 10.1039/c3sm52089g.

22 A. Alicke and J. Vermant, Yielding of model particle-laden interfaces in shear and compression, *Rheol. Acta*, 2025, **64**, 583–600, DOI: 10.1007/s00397-025-01524-9.

23 P. J. Beltramo, M. Gupta, A. Alicke, I. Liascukiene, D. Z. Gunes, C. N. Baroud and J. Vermant, Arresting dissolution by interfacial rheology design, *Proc. Natl. Acad. Sci. U. S. A.*, 2017, **114**(39), 10373–10378, DOI: 10.1073/pnas.1705181114.

24 M. E. H. van den Berg, S. Kuster, E. J. Windhab, L. M. C. Sagis and P. Fischer, Nonlinear shear and dilatational rheology of viscoelastic interfacial layers of cellulose nanocrystals, *Phys. Fluids*, 2018, **30**(7), 072103, DOI: 10.1063/1.5035334.

25 H. Zhang, K. Yu, O. J. Cayre and D. Harbottle, Interfacial Particle Dynamics: One and Two Step Yielding in Colloidal Glass, *Langmuir*, 2016, **32**(50), 13472–13481, DOI: 10.1021/acs.langmuir.6b03586.

26 A. Maestro and A. Zaccone, Nonaffine deformation and tunable yielding of colloidal assemblies at the air-water interface, *Nanoscale*, 2017, **9**(46), 18343–18351, DOI: 10.1039/c7nr06014a From NLM PubMed-not-MEDLINE.

27 J. D. Ferry, *Viscoelastic properties of polymers*, John Wiley & Sons, 1980.

28 M. Baumgaertel and H. H. Winter, Interrelation between continuous and discrete relaxation time spectra, *J. Non-Newtonian Fluid Mech.*, 1992, **44**, 15–36, DOI: 10.1016/0377-0257(92)80043-W.

29 M. Baumgaertel and H. H. Winter, Determination of discrete relaxation and retardation time spectra from dynamic mechanical data, *Rheol. Acta*, 1989, **28**(6), 511–519, DOI: 10.1007/bf01332922.

30 M. Baumgaertel, A. Schausberger and H. H. Winter, The relaxation of polymers with linear flexible chains of uniform length, *Rheol. Acta*, 1990, **29**(5), 400–408, DOI: 10.1007/bf01376790.

31 M. Siebenbürger, M. Fuchs, H. Winter and M. Ballauff, Viscoelasticity and shear flow of concentrated, noncrystallizing colloidal suspensions: Comparison with mode-coupling theory, *J. Rheol.*, 2009, **53**(3), 707–726, DOI: 10.1122/1.3093088 (acccessed 1/28/2025).

32 D. Renggli, A. Alicke, R. H. Ewoldt and J. Vermant, Operating windows for oscillatory interfacial shear rheology, *J. Rheol.*, 2020, **64**(1), 141–160, DOI: 10.1122/1.5130620.

33 H. H. Winter, Analysis of dynamic mechanical data: inversion into a relaxation time spectrum and consistency check, *J. Non-Newtonian Fluid Mech.*, 1997, **68**(2), 225–239, DOI: 10.1016/S0377-0257(96)01512-1.

34 C. Liu, J. He, E. V. Ruymbeke, R. Keunings and C. Bailly, Evaluation of different methods for the determination of the plateau modulus and the entanglement molecular weight, *Polymer*, 2006, **47**(13), 4461–4479, DOI: 10.1016/j.polymer.2006.04.054.

35 S. T. Milner and T. C. B. McLeish, Reptation and Contour-Length Fluctuations in Melts of Linear Polymers, *Phys. Rev. Lett.*, 1998, **81**(3), 725–728, DOI: 10.1103/PhysRevLett.81.725.

36 A. E. Likhtman and T. C. B. McLeish, Quantitative Theory for Linear Dynamics of Linear Entangled Polymers, *Macromolecules*, 2002, **35**(16), 6332–6343, DOI: 10.1021/ma0200219.

37 B. Xu and G. B. McKenna, Evaluation of the Dyre shoving model using dynamic data near the glass temperature, *J. Chem. Phys.*, 2011, **134**(12), 124902, DOI: 10.1063/1.3567092(acccessed 1/28/2025).

38 H. H. Winter, M. Siebenbürger, D. Hajnal, O. Henrich, M. Fuchs and M. Ballauff, An empirical constitutive law for concentrated colloidal suspensions in the approach of the glass transition, *Rheol. Acta*, 2009, **48**(7), 747–753, DOI: 10.1007/s00397-009-0377-5.

39 J. D. Peterson, W. Zou, R. G. Larson and M. E. Cates, Wormlike Micelles revisited: A comparison of models for linear rheology, *J. Non-Newtonian Fluid Mech.*, 2023, **322**, 105149, DOI: 10.1016/j.jnnfm.2023.105149.

40 L. Poh, E. Narimissa, M. H. Wagner and H. H. Winter, Interactive Shear and Extensional Rheology—25 years of IRIS Software, *Rheol. Acta*, 2022, **61**(4–5), 259–269, DOI: 10.1007/s00397-022-01331-6.

41 E. L. Correia, H. H. Winter and S. Razavi, Two-dimensional glass transition-like behavior of Janus particle-laden interface, *Rheol. Acta*, 2023, **62**(4), 239–251, DOI: 10.1007/s00397-023-01389-w.

42 E. B. Oliveira, E. L. Correia and S. Razavi, Wettability Effects on Interfacial Rheology and Stability of Particle-Laden Oil-Water Interfaces, *J. Colloid Interface Sci.*, 2026, **713**, 140144.

43 A. Dani, M. Yeganeh and C. Maldarelli, Hydrodynamic interactions between charged and uncharged Brownian colloids at a fluid–fluid interface, *J. Colloid Interface Sci.*, 2022, **628**(Pt B), 931–945, DOI: 10.1016/j.jcis.2022.08.084 From NLM Medline.